Toward a comprehensive description of decay properties for uranium isotopes

Yibin Qian[1,2,*] and Zhongzhou Ren[2,3,4,†]

[1]*Department of Applied Physics, Nanjing University of Science and Technology, Nanjing 210094, China*

[2]*Key Laboratory of Modern Acoustics and Department of Physics, Nanjing University, Nanjing 210093, China*

[3]*Kavli Institute for Theoretical Physics China, Beijing 100190, China*

[4]*Center of Theoretical Nuclear Physics, National Laboratory of Heavy-Ion Accelerator, Lanzhou 730000, China*

(Received 12 October 2016; published 27 December 2016)

Within the enhanced density dependent cluster model, with specific concern for density distributions in related nuclei, we investigate α decay and cluster radioactivity in uranium isotopes in the range $217 \leqslant A \leqslant 243$. The available experimental data are found to be well reproduced, especially including the very recently measured values of new neutron-deficient isotopes. The half-lives of possible cluster emissions are consequently predicted as well, and will be somewhat valuable for future detection. Moreover, β decay half-lives of these nuclei are also evaluated with respect to all kinds of β processes, while their spontaneous fission lifetimes are provided via an effective relationship between the half-life and crucial quantities, namely the fissility parameter and fission barriers. In this sense, a full understanding of decay properties in uranium isotopes is expected to be achieved by combining their various radioactive features.

DOI: 10.1103/PhysRevC.94.064321

I. INTRODUCTION

Dating back to early stages of nuclear physics, it was a uranium salt that triggered the discovery of radioactivity, leading to the entrance of nuclear physics into the field of natural science. Up to now, a series of unstable uranium isotopes, mostly decaying via α transitions, have been reported and synthesized, which has played an important role in both nuclear structural studies and nuclear energy applications [1–6]. Very recently, special attention has been devoted to very neutron-deficient uranium isotopes, in order to probe the structural evolution trend and to find their similarities, in analogy with isotonic nuclei [2,3]. Moreover, two short-lived isotopes ^{221,222}U beyond the $N = 126$ neutron shell were recently studied for a new perspective on the weakening of the shell effect in a relatively-open shell region [4]. Besides, whether the shell gap at $Z = 92$ iexists can be determined through the decay of low-lying states in ^{218}U [5]. It is important to recall that these structural phenomena were all revealed via α decay spectra, and even the energy levels of their products can be identified correspondingly [6]. On the other hand, since the experimental efforts to find cluster emitters in the 1980s, several uranium isotopes have been confirmed to carry cluster radioactivity, increasing the number of the fifamily members showing this rare decay mode [1]. In this sense, these heavy nuclei with $Z = 92$ provide a suitable factory for us to detect α or heavier cluster emission.

Since Gamow's explanation of α (or cluster) decay as a quantum tunneling phenomenon, α decay is usually taken to be a two-step process, i.e., the preformation of the emitted particle and its penetration through the potential barrier. Accordingly, extensive studies have been devoted to the successful description of α (cluster) decay during the past decades [7–20], on the basis of various models such as the shell model, the cluster model, and the fissionlike model. Several effective formulas, similar to the famous Geiger-Nuttall law, have been also proposed to evaluate α decay half-lives by including key ingredients [15,21–24]. Besides, the fine structure of α decay has been systematically investigated within the coupled-channel approach for a large range of nuclei [25,26]. In our recent studies, α particle and heavier cluster decay have been both reexamined within an improved cluster model [27,28], where the essential potential is constructed based on the specific density distributions of required nuclei from the data of nuclear radii. The enhanced calculation is then expected to be more reasonable and reliable, and the important cluster-preformation probability appears to behave differently as compared to previous thought. Apparently, the aforementioned experimental data give us a perfect opportunity to check the developed model, while the theoretical results may in turn validate the accuracy of the new measurement. As a further step, another objective of this work is aimed at hitherto unknown decay features of uranium isotopes. To accomplish this goal, other possible decay channels of uranium isotopes should also receive attention.

According to the available experimental analyses and theoretical studies [1,17,29,30], β decay and spontaneous fission could be involved in the decays of uranium isotopes. Although spontaneous fission (SF) has a mechanism similar to α or cluster radioactivity, a fully realistic depiction of SF is still a quite difficult task, and seems to be restricted to certain typical nuclei due to the requirements of detailed knowledge of the multidimensional potential energy surface plus the collective inertia [29]. Meanwhile, the fissility parameter should be sensitively connected to the SF half-life (T_{sf}), and the barrier height of the potential energy surface is believed to determine T_{sf} as well. With this in mind, we employ an effective systematics [29] combined with these two quantities to estimate the SF lifetime in a convenient and reliable way. Regarding β decay, in addition to the useful phenomenological

*qyibin@njust.edu.cn

†zren@nju.edu.cn

relations, microscopic calculations generally come down to the rather complicated and time-consuming computation of the corresponding transition matrix element [17,30]. Because the matrix element is approximately a constant for one kind of β decay, the estimation of β decay half-life can be reduced to the calculation of the Fermi function. Here we will use this method and the NRV code [31]. More importantly, the branching ratios of β decay and SF of the considered isotopes are believed to be satisfactorily determined in this way. Consequently, the present evaluation can reasonably produce the general trend in the decay modes, which is interesting and valuable for us.

The organization of this paper is as follows. The theoretical approach for obtaining the half-lives of α decay and cluster radioactivity is briefly presented in Sec. II. In Section III, the employed systematics of β decay and spontaneous fission is initially described, and the detailed results including complete predictions are tabulated and describeed. After the corresponding discussions, a summary is given in Sec. IV.

II. THEORETICAL FRAMEWORK

A. Density dependent cluster model with refined density distributions of nuclei

As mentioned previously, the α or heavier cluster decay process is usually assumed as a preformed cluster tunneling through the potential barrier between the cluster and the residual daughter nucleus. At this point, the decaying parent nucleus can be considered as a cluster (including α particle or heavier cluster) plus core system, where the interaction potential between the two components is fundamental and crucial for the calculation of decay half-life. When it comes to the specific calculation, the radial Schrödinger equation for the cluster-core relative motion should be solved within the total potential composed of nuclear and Coulomb parts plus the centrifugal term, namely

$$V(r) = \lambda V_N(r) + V_C(r) + \frac{\ell(\ell+1)\hbar^2}{2\mu r^2}. \tag{1}$$

The λ is the renormalization factor for the depth of the nuclear potential, μ is the reduced mass of the cluster-core system measured in units of nucleon mass $\mu = \frac{A_c A_d}{A_c + A_d}$, and ℓ is the angular momentum carried by the emitted cluster. In this study, the nuclear and Coulomb potentials are built by the double folding integral of the respective density distributions of the cluster and the core nucleus and the corresponding nucleon-nucleon (NN) interaction [32–34]:

$$V_{Nor\,C}(\mathbf{r}) = \iint d\mathbf{r_1} d\mathbf{r_2} \left[\rho_1^n(\mathbf{r_1}) + \rho_1^p(\mathbf{r_1})\right]\left[\rho_2^n(\mathbf{r_2}) + \rho_2^p(\mathbf{r_2})\right] \times \upsilon(\mathbf{s} = |\mathbf{r_2} + \mathbf{r} - \mathbf{r_1}|), \tag{2}$$

Besides the separation distance r between the mass centers of the cluster and the core, $\upsilon(\mathbf{s})$ is the standard proton-proton Coulomb interaction for the Coulomb potential. As for the nuclear potential, the NN interaction $\upsilon(\mathbf{s})$ is chosen to be of the effective M3Y-Reid type, widely used in nuclear radioactivity [9,26] and reaction studies [32–34]. The specific formulas and computation details can be found in Refs. [9,26,32–34] and references therein. The density distributions of the daughter nucleus (ρ_1) are given by the popular two-parameter Fermi (2pF) form,

$$\rho_1^\xi(r_1) = \frac{\rho_0^\xi}{1 + \exp\left(\frac{r_1 - R_{1/2}^\xi}{a^\xi}\right)}, \tag{3}$$

where ξ is p or n, and the ρ_0 value is determined by integrating the density distribution equivalent to the proton or neutron number of the corresponding nucleus. The half-density radius $R_{1/2}$ is connected with the mass number of related nuclei via $R_{1/2} = c^\xi A^{1/3}$. The details of choosing the parameters c^ξ and a^ξ will be presented in the next subsection; meanwhile they can be obtained via the relationship between the rms proton and neutron radii of nuclei and the density distribution:

$$R^\xi \equiv \sqrt{\langle r^2 \rangle} = \left[\frac{\int \rho(r) r^4 dr}{\int \rho(r) r^2 dr}\right]^{1/2}. \tag{4}$$

After the required nuclear and Coulomb potentials are constructed within the above process, the following procedure proceeds via the solution of the aforementioned stationary Schrödinger equation against the cluster-core system:

$$\left(-\frac{\hbar^2}{2\mu}\frac{d^2}{dr^2} + V(r)\right)\varphi_{n\ell j}(r) = Q\varphi_{n\ell j}(r). \tag{5}$$

Note that the renormalization factor λ is settled to adjust the experimental decay energy Q, due to the fact that the calculated decay width is very sensitive to the Q value and the accuracy of Q cannot be sufficiently predicted in a given potential. To account for the effect of the Pauli principle, the quantum number n (indicating the number of the internal nodes in the radial wave function) is determined by the Wildermuth and Tang condition [35],

$$G = 2n + L = \sum_{i=1}^{A_c} \left(g_i^{A_c + A_d} - g_i^{A_c}\right), \tag{6}$$

during this calculatiion process. In this expression, $g_i^{A_c+A_d}$ is the oscillator quantum number in the parent nucleus for the ingredient nucleons of the cluster, and its value is required to guarantee the cluster is completely outside the shell occupied by the daughter nucleus. On the other hand, $g_i^{A_c}$ is the interior quantum number of the cluster in the shell-model picture. It should be noted that the latter quantum number is actually zero when the cluster is α particle. The quantum numbers of the cluster above the core are then related to the inner quantum numbers of the nucleons forming the cluster. Here we take $g_i = 6$ for nucleons beyond the $N = 126$ shell closure, $g_i = 5$ for nucleons in the $82 < Z,N \leqslant 126$ shell, and $g_i = 4$ for nucleons in the $50 < Z,N \leqslant 82$ shell. In this way, the radial wave function $\varphi_{n\ell j}(r)$ can be obtained by solving the Schrödinger equation with the outgoing Coulomb wave-function boundary condition [25,26,36]

$$\varphi_{n\ell j}(r) = N_{\ell j}[G_\ell(kr) + iF_\ell(kr)], \tag{7}$$

where $N_{\ell j}$ is the normalization constant, and G_ℓ and F_ℓ are respectively the irregular and regular Coulomb wave functions with wave number $k = \sqrt{2\mu Q}/\hbar$. Subsequently, the

probability rate per second that the particle goes through a sphere is given by integrating $|\varphi_{n\ell j}(r)|^2 v \sin\theta\, d\theta\, d\phi$ over the angles where the velocity of the particle at large distances is $v = \hbar k/\mu$. Given that $|\varphi_{n\ell j}(r)|^2 = |N_{\ell j}|^2$ at the large distance R and the inner and outer wave functions should matched, one can obtain the decay width as [25,26,36]

$$\Gamma = \frac{\hbar^2 k}{\mu}|N_{\ell j}|^2 = \frac{\hbar^2 k}{\mu}\frac{|\varphi_{n\ell j}(R)|^2}{G_\ell(kR)^2 + F_\ell(kR)^2}, \tag{8}$$

which yields almost the same value despite different choices of R beyond the range of the nuclear potential. The half-life can be ultimately obtained via the well-known relationship

$$T_{1/2} = \frac{\hbar \ln 2}{P_c \Gamma}, \tag{9}$$

where P_c is the cluster preformation factor, presenting the formation probability of an emitted cluster at the surface of a parent nucleus. There is no doubt that this quantity is indispensable for calculating the absolute half-life value. Considering that the preformation factor of α decay varies in general smoothly in the open shell region from the experimental aspect, while its microscopic calculation appears to be extremely difficult, the P_α value can be approximately taken as constant for one kind of nuclei to minimize the number of parameters. Actually, these α-preformation factors of heavy nuclei still fluctuate, especially dramatically in the closed-shell region due to the shell effect, as can be seen from the specific results in the cluster-formation model [37] and the extraction procedure plus the analytical expression based on the experimental data [16,38]. In this study, the α-preformation factor is determined by fitting the available experimental half-lives, and the influence of the $N = 126$ shell on the preformation factor will be discussed somewhat in the next section. When it comes to heavier cluster emission, the situation appears to be more complicated, and our previous treatment is used via the formula,

$$\log_{10} P_c = a\sqrt{\mu}(Z_c Z_d)^{1/2} + b, \tag{10}$$

which is based on the direct recognition that the formation of a cluster should be largely affected by its own dimension and the size of the parent nucleus. Here Z_c and Z_d are the atomic numbers of the cluster and the daughter nucleus, while the parameters a,b are to be fixed.

One can see that several parameters are involved in the calculation, and specific choices about them will be discussed in the next part. Before that, we take into account the influence of nuclear deformation (deviation from spherical symmetry) on the α decay process. The daughter nuclei generally locate around the doubly magic nucleus ^{208}Pb and behave as spherical or nearly spherical shapes for cluster radioactivity, whereas the heavy nuclei in α decay mostly have deformed shapes. Therefore, the daughter nuclei of α decay are assumed to be of axial-symmetric type, and identical 2pF behavior, but with an orientation-dependent half-density radius,

$$R_{1/2}(\theta) = cA_1^{1/3}[1 + \beta_2 Y_{20}(\theta) + \beta_4 Y_{40}(\theta)], \tag{11}$$

is employed to depict their density distributions. The β_2 and β_4 are the quadrupole and hexadecapole deformation parameters, which are taken from the recent theoretical values in the finite-range droplet model [39]. Then, the orientational double-folding potential can be evaluated via the sum of different multipole components after the adoption of the multipole expansion for the deformed density distribution (see Refs. [26,34] and references therein). Considering that the emitted particle could be in any direction θ_1 with respect to the symmetrical axis of the daughter nucleus, one can obtain the partial decay width $\Gamma(\theta_1)$ for one certain orientation angle through the above procedure. At last, the final decay width can be achieved by averaging the partial decay width over all directions.

B. Parameter choice in the calculation

As illustrated above, the specific parameters involved in the density distribution are crucial for the following computation due to the significant dependence of the nuclear potential on the density distribution. Previously, these parameters were usually chosen to be the standard values in the literature [40,41], though they appear to be closely connected with the nuclear radii as well. Meanwhile, there have been quite a few experimental radii data accumulated, especially for the presently considered nuclei. We choose to obtain these parameters from the experimental nuclear radii instead of the standard values [27,28,42]. More importantly, the proton and neutron density distributions of daughter nuclei should be separately accounted for in terms of the phenomenon of neutron skin. Referring to the thickness of neutron skin, two extreme cases, namely the "neutron skin" type and the "neutron halo" type, have been adopted to describe the difference between the root-mean-square (rms) neutron radius and the rms proton radius, i.e., $\Delta R_{np} = R_n - R_p$ [43,44]. It should be noted that the final calculated results are quite close to each other, regardless of density distribution type [28,42]. With this in mind, we prefer to use the "neutron halo" type in the 2pF density distribution, which has relatively preferential support of the antiprotonic atom experiment [44,45]. In detail, for the "halo" type of nuclei, the diffuseness parameter a in the proton density distribution is still fixed at the standard value $a^p = 0.54$ fm, while the half-density radius parameter c^p is determined according to the the measured charge radii or the corresponding systematics [46]. Then, the diffuseness parameter a^n in the neutron density distribution can be obtained from the rms neutron radius, $R_n = R_p + \Delta R_{np}$, within the same half-density parameter $c^n = c^p$. Up to now, the effective measurement of rms nuclear neutron radii has been restricted, with relatively large error bars [45,47], although a number of experimental data on nuclear charge radii have been reported via various efficient tools [46]. Despite the limited experimental value of R_n and the uncertainties, the neutron skin thickness ΔR_{np} is found to behave in a linear relationship with the neutron-proton asymmetry term $I = (N - Z)/A$, which is consistent with other theoretical predictions [43,44]. This linear relationship is expressed as $\Delta R_{np} = (0.90 \pm 0.15)I + (-0.03 \pm 0.02)$ fm, populating the coherent value $\Delta R_{np} = 0.160(52)$ fm with both the available experimental data and theoretical results for ^{208}Pb. Encouraged

by this, we employ this simple and reliable expression to evaluate the thickness of the neutron skin.

After the cluster-core potential is obtained by using the above density distribution, the decay width can be provided through the above procedure. Consequently, the cluster preformation factor is needed to achieve the final half-life, as shown in Eq. (9). The general treatment of this quantity was presented in the preceding section, and their specific parameter values will be introduced in the following. On one hand, the α-preformation factor is determined by a least-squares fit to the available experimental data, namely $P_\alpha^{e\text{-}e} = 0.167$ and $P_\alpha^{\text{odd-}A} = 0.0915$, in the present study. On the other hand, considering the block effect of the unpaired nucleon on the cluster preformation process for odd-A nuclei, there exist different hindrances in even-even and odd-A heavier cluster emitters. To account for these different hindrances in a direct and consistent way, the parameter a in Eq. (10) maintains the same value for even-even and odd-A nuclei while the b value behaves differently for the systematic study of all kinds of emitters. Through a fitting process of the P_c value, as mentioned in Ref. [28], the experimental half-lives of available cluster emitters can be well reproduced by the following parameters:

$$\begin{aligned} a &= -0.065, \\ b^{e\text{-}e} &= 1.809, \\ b^{\text{odd-}A} &= 0.660. \end{aligned}$$

Interestingly, if the parameters a and b are not determined in the above way (fixed a for odd-A nuclei, the same as that of even-even ones) but are separately fixed from the fitting process for different kinds of nuclei, their values are still the same as the above ones. Consequently, we may conclude that this treatment dealing with the hindrance factor b is convincing and reasonable.

III. NUMERICAL RESULTS AND DISCUSSIONS

To give a broad picture of decay properties in uranium isotopes, we take account into their β decay and spontaneous fission in the meantime. According to the formulas and notations in Refs. [29,31] and references therein, we regard the β decay half-life with respect to all kinds of β processes as

$$\frac{1}{T_{1/2}^{\beta}} = \frac{1}{T_{1/2}^{\beta^+}} + \frac{1}{T_{1/2}^{\beta^-}} + \frac{1}{T_{1/2}^{EC}}, \tag{12}$$

with the following relations:

$$\begin{aligned} T_{1/2}^{b} &= \left(\sum_{E_f < Q_b} \frac{1}{t} \right)^{-1}, \\ f_0^b t &= \left(\frac{g^2 m_e^5 c^4}{2\pi^3 \hbar^7} |M_{if}|^2 \right)^{-1}, \end{aligned} \tag{13}$$

where b indicates $\beta^\pm$ or electron capture (EC), M_{if} is corresponding transition matrix element between the initial (i) and final (f) states, and t is the partial decay time to the final state f. Notice that the summation will be done over all energetically allowed states in the daughter nucleus. As is known, the $f_0^b t$ value can approximately be assumed to be one constant for each kind of β decay. Hence the evaluation of β decay half-lives is reduced to the computation of the Fermi function f_0^b, which is obtained via the code NRV [31] here. Besides β decay, for the sake of convenience and reliability, an effective relationship is given by [29]

$$\begin{aligned} \log_{10} T_{1/2}^{SF} = {} & 1146.44 - 75.3153 Z^2/A + 1.63792 (Z^2/A)^2 \\ & - 0.0119827 (Z^2/A)^3 + B_f (7.23613 \\ & - 0.0947022 Z^2/A) \\ & + \begin{cases} 0, & \text{even-even nuclei,} \\ 1.53897, & \text{odd-A nuclei,} \\ 0.80822, & \text{odd-odd nuclei,} \end{cases} \end{aligned} \tag{14}$$

where the SF half-life is related to the fissility parameter and the important fission barrier height B_f. The results of this expression are not only in good agreement with the available experimental data but also vary similarly with the dynamical predictions [29], which supports our current work to a great extent. The fully microscopic description of these two decay modes, namely β decay and SF process, is out of the present scope. Furthermore, the present evaluation of their lifetimes in this study is expected to be capable of providing enough knowledge of the stability against the concerned decay channels via their competition. With the consideration of the two additional decay modes, we systematically investigate the decay properties of uranium isotopes including related predictions of future measurement.

Table I represents the detailed results of half-lives for α and heavier particle emission, compared with the available experimental data. The first column denotes the specific transition involving the parent and daughter nuclei and the emitted cluster. The experimental decay energy and half-life, mainly taken from Refs. [1,48], are shown in the second and third columns. The calculated half-lives in the present model are given in the fourth column. In addition, the evaluated results via the unified formula of half-lives for α decay and cluster emission [22,24],

$$\log_{10} T_{1/2} = c_1 \sqrt{\mu} Z_c Z_d Q^{-1/2} + c_2 \sqrt{\mu} (Z_c Z_d)^{1/2} + c_3 \tag{15}$$

with the fitted parameters, are listed in the last column for comparison. As one can see from the table, our calculated results are in good agreement with the experimental ones, for any α decay or heavier cluster emission. Notably, the measured values of newly reported neutron-deficient isotopes ^{215,216}U [2,3] and near-shell nuclei ^{221,222}U are well described, to further check the validity of the present approach. More importantly, the vital α-preformation factor, as the significant hint of the shell effect, is taken as one identical constant over all the studied region. Regardless of this, the calculated half-lives of $^{215\text{–}222}$U close to the neutron shell $N = 126$ are still found to be totally consistent with the measured values, whereas the shell effect is supposed to yield clear deviations between theory and experiment. This implies that the influence of the

TABLE I. Comparison of calculated half-lives in the present model with available experimental data for cluster emissions in various U isotopes, including α decay and heavier cluster radioactivity. Besides the nuclear database [1,48], new or improved experimental data (denoted by symbol "*") are taken from Refs. [2–4,6]. Note that the unified formula [22,24] of α decay and cluster radioactivity half-lives is also employed to provide referenced results in the last column.

Transition	Q (MeV)	$T_{1/2}^{\rm expt}$	$T_{1/2}^{\rm calc}$	$T_{1/2}^{\rm form}$
$^{*215}\mathrm{U} \rightarrow {}^{211}\mathrm{Th} + \alpha$	8.588	$0.73^{+1.33}_{-0.29}$ ms	2.79 ms	3.52 ms
$^{*216}\mathrm{U} \rightarrow {}^{212}\mathrm{Th} + \alpha$	8.542	$4.72^{+4.72}_{-1.57}$ ms	1.99 ms	0.86 ms
$^{218}\mathrm{U} \rightarrow {}^{214}\mathrm{Th} + \alpha$	8.773	$0.51^{+0.17}_{-0.10}$ ms	0.40 ms	0.19 ms
$^{219}\mathrm{U} \rightarrow {}^{215}\mathrm{Th} + \alpha$	9.860	42^{+34}_{-13} μs	14 μs	13 μs
$^{*221}\mathrm{U} \rightarrow {}^{217}\mathrm{Th} + \alpha$	9.889	0.66 ± 0.14 μs	0.59 μs	1.73 μs
$^{*222}\mathrm{U} \rightarrow {}^{218}\mathrm{Th} + \alpha$	9.481	4.7 ± 0.7 μs	2.8 μs	2.9 μs
$^{223}\mathrm{U} \rightarrow {}^{219}\mathrm{Th} + \alpha$	8.940	55 ± 10 μs	117 μs	383 μs
$^{224}\mathrm{U} \rightarrow {}^{220}\mathrm{Th} + \alpha$	8.633	409.9 ± 17.6 μs	429.4 μs	476.3 μs
$^{225}\mathrm{U} \rightarrow {}^{221}\mathrm{Th} + \alpha$	8.009	83 ± 18 ms	98 ms	191 ms
$^{226}\mathrm{U} \rightarrow {}^{222}\mathrm{Th} + \alpha$	7.702	316 ± 7 ms	303 ms	337 ms
$^{*227}\mathrm{U} \rightarrow {}^{223}\mathrm{Th} + \alpha$	6.987	2.2 ± 0.1 min	3.6 min	11.5 min
$^{228}\mathrm{U} \rightarrow {}^{224}\mathrm{Th} + \alpha$	6.799	13.3 ± 0.3 min	10.9 min	11.4 min
$^{229}\mathrm{U} \rightarrow {}^{225}\mathrm{Th} + \alpha$	6.473	453.1 ± 23.4 min	482.4 min	1461 min
$^{230}\mathrm{U} \rightarrow {}^{226}\mathrm{Th} + \alpha$	5.993	30.86 ± 3.12 d	33.22 d	29.10 d
$^{232}\mathrm{U} \rightarrow {}^{228}\mathrm{Th} + \alpha$	5.356	101.1 ± 0.6 y	218.2 y	185.5 y
$^{233}\mathrm{U} \rightarrow {}^{229}\mathrm{Th} + \alpha$	4.908	1.89×10^5 y	2.78×10^5 y	5.83×10^5 y
$^{234}\mathrm{U} \rightarrow {}^{230}\mathrm{Th} + \alpha$	4.858	3.44×10^5 y	3.11×10^5 y	2.26×10^5 y
$^{235}\mathrm{U} \rightarrow {}^{231}\mathrm{Th} + \alpha$	4.472	1.22×10^9 y	4.76×10^8 y	6.88×10^8 y
$^{236}\mathrm{U} \rightarrow {}^{232}\mathrm{Th} + \alpha$	4.571	3.17×10^7 y	3.49×10^7 y	2.26×10^7 y
$^{238}\mathrm{U} \rightarrow {}^{234}\mathrm{Th} + \alpha$	4.270	5.66×10^9 y	9.99×10^9 y	4.69×10^9 y
$^{230}\mathrm{U} \rightarrow {}^{208}\mathrm{Pb} + {}^{22}\mathrm{Ne}$	61.39	3.72×10^{19} s	3.09×10^{19} s	1.23×10^{20} s
$^{232}\mathrm{U} \rightarrow {}^{208}\mathrm{Pb} + {}^{24}\mathrm{Ne}$	62.31	2.45×10^{20} s	4.17×10^{20} s	2.29×10^{20} s
$^{233}\mathrm{U} \rightarrow {}^{209}\mathrm{Pb} + {}^{24}\mathrm{Ne}$	60.49	6.92×10^{24} s	2.63×10^{24} s	2.51×10^{24} s
$^{233}\mathrm{U} \rightarrow {}^{208}\mathrm{Pb} + {}^{25}\mathrm{Ne}$	60.78	6.92×10^{24} s	3.98×10^{24} s	6.76×10^{24} s
$^{234}\mathrm{U} \rightarrow {}^{210}\mathrm{Pb} + {}^{24}\mathrm{Ne}$	58.83	8.51×10^{25} s	6.03×10^{25} s	6.31×10^{25} s
$^{234}\mathrm{U} \rightarrow {}^{208}\mathrm{Pb} + {}^{26}\mathrm{Ne}$	59.47	8.51×10^{25} s	1.58×10^{26} s	3.24×10^{26} s
$^{234}\mathrm{U} \rightarrow {}^{206}\mathrm{Hg} + {}^{28}\mathrm{Mg}$	74.11	3.39×10^{25} s	2.95×10^{25} s	1.82×10^{25} s

$N = 126$ shell closure begins to gradually fade in U isotopes, which is exactly consistent with the indication of Ref. [4].

Encouraged by the excellent agreement, possible cluster emissions of U are predicted with the help of nuclear masses from Ref. [1]. On one hand, a few hitherto unknown α-decaying nuclei are predicted, along with a strongly recommended candidate ^{217}U. Actually, there have already been experiments aimed at this nucleus. However, the existing data appear to be still inconclusive [1], and the prediction here is expected to be helpful for the further experiments on ^{217}U. On the other hand, we also pay a great deal of attention to the cluster emission, which indeed occurs in uranium isotopes. In view of available knowledge about cluster emission, the daughter nuclei usually locate around the magic nucleus, i.e. lead isotopes. In addition, cluster emission of uranium isotopes decaying to even-Z products, namely Hg and Pb isotopes, releases much more energy compared to that leading to neighboring odd-Z Tl and Bi nuclei, according to our calculation. Meanwhile, the decay transition from the even-Z parent nucleus should be in favor of an even-Z daughter, otherwise the difference between parent and daughter could result in structural hindrance in terms of the centrifugal potential and cluster preformation factor. This intuitive fact can be taken as further evidence to make us focus on the transition from U to Hg and Pb, which is specifically demonstrated in Table II.

As clearly shown, the half-lives of cluster radioactivity are generally beyond the α decay ones in quite large orders of magnitude. Consequently, uranium isotopes will rarely decay via cluster emission, and this decay mode should only possess a tiny branch ratio. When the isotopes approach the neutron-deficient or neutron-rich side, β decay begins to play a significant role in their decay routes. Specifically, β^- decay should dominate in the neutron-rich isotopes while β^+ decay is more favorable in the neutron-deficient region.

As mentioned before, all kinds of β decay are considered here to obtain the total half-lives. The comparison of calculated β decay half-lives with the available experimental data is displayed in Table III, containing several predictions on β decay half-lives. As for the absent U isotopes, most of them

TABLE II. Predictions on unknown half-lives of α decay and cluster radioactivity for uranium isotopes in logarithm scale, including the empirical evaluations as in Table I.

Transition	Q (MeV)	$\log_{10} T_{1/2}^{\rm calc}$ (s)	$\log_{10} T_{1/2}^{\rm form}$ (s)
$^{217}\mathrm{U} \rightarrow {}^{213}\mathrm{Th} + \alpha$	8.430	−1.88	−2.00
$^{220}\mathrm{U} \rightarrow {}^{216}\mathrm{Th} + \alpha$	10.210	−7.19	−7.23
$^{239}\mathrm{U} \rightarrow {}^{235}\mathrm{Th} + \alpha$	4.131	18.95	19.07
$^{240}\mathrm{U} \rightarrow {}^{236}\mathrm{Th} + \alpha$	4.036	19.53	19.14
$^{241}\mathrm{U} \rightarrow {}^{237}\mathrm{Th} + \alpha$	3.820	21.86	21.87
$^{242}\mathrm{U} \rightarrow {}^{238}\mathrm{Th} + \alpha$	3.570	24.25	23.64
$^{243}\mathrm{U} \rightarrow {}^{239}\mathrm{Th} + \alpha$	3.370	26.83	26.59
$^{217}\mathrm{U} \rightarrow {}^{197}\mathrm{Pb} + {}^{20}\mathrm{Ne}$	54.76	32.11	29.62
$^{217}\mathrm{U} \rightarrow {}^{193}\mathrm{Hg} + {}^{24}\mathrm{Mg}$	67.97	35.83	32.08
$^{218}\mathrm{U} \rightarrow {}^{196}\mathrm{Pb} + {}^{22}\mathrm{Ne}$	55.30	32.31	29.61
$^{218}\mathrm{U} \rightarrow {}^{194}\mathrm{Hg} + {}^{24}\mathrm{Mg}$	68.03	34.51	30.74
$^{219}\mathrm{U} \rightarrow {}^{197}\mathrm{Pb} + {}^{22}\mathrm{Ne}$	56.03	32.05	29.58
$^{219}\mathrm{U} \rightarrow {}^{193}\mathrm{Hg} + {}^{26}\mathrm{Mg}$	70.57	33.51	29.95
$^{220}\mathrm{U} \rightarrow {}^{198}\mathrm{Pb} + {}^{22}\mathrm{Ne}$	57.00	29.04	26.78
$^{220}\mathrm{U} \rightarrow {}^{194}\mathrm{Hg} + {}^{26}\mathrm{Mg}$	71.33	30.97	27.58
$^{221}\mathrm{U} \rightarrow {}^{199}\mathrm{Pb} + {}^{22}\mathrm{Ne}$	57.74	28.90	26.86
$^{221}\mathrm{U} \rightarrow {}^{195}\mathrm{Hg} + {}^{26}\mathrm{Mg}$	71.69	31.55	28.32
$^{222}\mathrm{U} \rightarrow {}^{200}\mathrm{Pb} + {}^{22}\mathrm{Ne}$	58.50	26.27	24.41
$^{222}\mathrm{U} \rightarrow {}^{196}\mathrm{Hg} + {}^{26}\mathrm{Mg}$	72.26	29.23	26.25
$^{223}\mathrm{U} \rightarrow {}^{201}\mathrm{Pb} + {}^{22}\mathrm{Ne}$	59.12	26.25	24.70
$^{223}\mathrm{U} \rightarrow {}^{197}\mathrm{Hg} + {}^{26}\mathrm{Mg}$	72.60	29.76	27.04
$^{224}\mathrm{U} \rightarrow {}^{202}\mathrm{Pb} + {}^{22}\mathrm{Ne}$	59.68	24.06	22.59
$^{224}\mathrm{U} \rightarrow {}^{198}\mathrm{Hg} + {}^{26}\mathrm{Mg}$	72.88	27.98	25.38
$^{225}\mathrm{U} \rightarrow {}^{203}\mathrm{Pb} + {}^{22}\mathrm{Ne}$	60.19	24.26	23.09
$^{225}\mathrm{U} \rightarrow {}^{199}\mathrm{Hg} + {}^{26}\mathrm{Mg}$	73.14	28.64	26.29
$^{226}\mathrm{U} \rightarrow {}^{204}\mathrm{Pb} + {}^{22}\mathrm{Ne}$	60.46	22.52	21.42
$^{226}\mathrm{U} \rightarrow {}^{198}\mathrm{Hg} + {}^{28}\mathrm{Mg}$	73.30	28.08	26.32
$^{227}\mathrm{U} \rightarrow {}^{205}\mathrm{Pb} + {}^{22}\mathrm{Ne}$	60.82	22.97	22.17
$^{227}\mathrm{U} \rightarrow {}^{199}\mathrm{Hg} + {}^{28}\mathrm{Mg}$	73.59	28.64	27.17
$^{228}\mathrm{U} \rightarrow {}^{206}\mathrm{Pb} + {}^{22}\mathrm{Ne}$	61.03	21.32	20.60
$^{228}\mathrm{U} \rightarrow {}^{200}\mathrm{Hg} + {}^{28}\mathrm{Mg}$	73.74	27.08	25.70
$^{229}\mathrm{U} \rightarrow {}^{207}\mathrm{Pb} + {}^{22}\mathrm{Ne}$	61.69	21.33	20.90
$^{229}\mathrm{U} \rightarrow {}^{201}\mathrm{Hg} + {}^{28}\mathrm{Mg}$	73.89	27.82	26.76
$^{231}\mathrm{U} \rightarrow {}^{207}\mathrm{Pb} + {}^{24}\mathrm{Ne}$	62.21	22.14	21.75
$^{231}\mathrm{U} \rightarrow {}^{203}\mathrm{Hg} + {}^{28}\mathrm{Mg}$	74.10	27.17	26.50
$^{235}\mathrm{U} \rightarrow {}^{209}\mathrm{Pb} + {}^{26}\mathrm{Ne}$	58.06	29.64	30.09
$^{235}\mathrm{U} \rightarrow {}^{207}\mathrm{Hg} + {}^{28}\mathrm{Mg}$	72.43	28.45	29.00
$^{235}\mathrm{U} \rightarrow {}^{206}\mathrm{Hg} + {}^{29}\mathrm{Mg}$	72.47	29.26	29.69
$^{236}\mathrm{U} \rightarrow {}^{210}\mathrm{Pb} + {}^{26}\mathrm{Ne}$	56.70	30.66	31.22
$^{236}\mathrm{U} \rightarrow {}^{206}\mathrm{Hg} + {}^{30}\mathrm{Mg}$	72.28	28.85	29.47
$^{237}\mathrm{U} \rightarrow {}^{211}\mathrm{Pb} + {}^{26}\mathrm{Ne}$	55.40	34.17	34.84
$^{237}\mathrm{U} \rightarrow {}^{207}\mathrm{Hg} + {}^{30}\mathrm{Mg}$	70.76	31.69	33.12
$^{238}\mathrm{U} \rightarrow {}^{212}\mathrm{Pb} + {}^{26}\mathrm{Ne}$	54.38	34.75	35.52
$^{238}\mathrm{U} \rightarrow {}^{208}\mathrm{Hg} + {}^{30}\mathrm{Mg}$	69.46	32.46	33.97
$^{239}\mathrm{U} \rightarrow {}^{213}\mathrm{Pb} + {}^{26}\mathrm{Ne}$	53.30	37.41	38.88
$^{239}\mathrm{U} \rightarrow {}^{209}\mathrm{Hg} + {}^{30}\mathrm{Mg}$	68.10	35.75	37.52
$^{240}\mathrm{U} \rightarrow {}^{214}\mathrm{Pb} + {}^{26}\mathrm{Ne}$	52.42	38.42	39.38
$^{240}\mathrm{U} \rightarrow {}^{210}\mathrm{Hg} + {}^{30}\mathrm{Mg}$	66.97	36.44	38.21
$^{241}\mathrm{U} \rightarrow {}^{215}\mathrm{Pb} + {}^{26}\mathrm{Ne}$	51.30	41.31	42.93
$^{241}\mathrm{U} \rightarrow {}^{211}\mathrm{Hg} + {}^{30}\mathrm{Mg}$	65.70	39.71	41.71
$^{242}\mathrm{U} \rightarrow {}^{216}\mathrm{Pb} + {}^{26}\mathrm{Ne}$	50.66	41.43	43.03
$^{242}\mathrm{U} \rightarrow {}^{210}\mathrm{Hg} + {}^{32}\mathrm{Mg}$	64.82	41.21	43.84
$^{243}\mathrm{U} \rightarrow {}^{217}\mathrm{Pb} + {}^{26}\mathrm{Ne}$	49.68	44.74	46.41
$^{243}\mathrm{U} \rightarrow {}^{211}\mathrm{Hg} + {}^{32}\mathrm{Mg}$	63.85	44.19	46.95

TABLE III. Calculated β decay half-lives versus the available experimental data, including several predictions. Some isotopes are not illustrated because most of them are forbidden in terms of their decay energies, and rest of them are ambiguously recognized in the spectrum scheme (important for the determination of the β decay process).

Parent	$T_{1/2}^{\mathrm{expt}}$	$T_{1/2}^{\mathrm{calc}}$
^{218}U		11.17 min
^{221}U		6.47 h
^{222}U	2.33 min	30.22 min
^{224}U	13.06 min	3.84 min
^{226}U		1.39 h
^{227}U	76.39 d	1.17 d
^{229}U	1.21 h	21.04 min
^{231}U	4.20 d	10.94 h
^{237}U	6.752 d	5.26 d
^{239}U	23.45 min	5.78 min
^{240}U	14.10 h	8.49 h
^{242}U	16.80 min	11.98 min

are forbidden in view of decay energy, while the residuals are not well fit into the spectroscopic scheme, resulting in the vagueness. It is found that the theoretical results of β decay are satisfactorily consistent with measurements, which somewhat validates the corresponding prediction as well. Notice that possible β decay channels ($\beta^{\pm}$ and EC) are all taken into account for one given nucleus, while the available experimental data are sometimes limited to one kind of process. Consequently, this would cause the slight deviation between calculated results and measured values, particularly for the nucleus ^{227}U. In fact, the calculated β^{+} decay half-life of this nucleus is 136.73 d, which is quite close to the corresponding experimental one, namely 76.39 d. Moreover, the experimental β decay half-lives of ^{222,227}U have been reported in Refs. [1,48] in a tentative way, which also emphasizes the deviations between theoretical calculations and experimental data to a certain extent.

Next, the spontaneous fission lifetimes of these studied isotopes are obtained via the relationship (14) to achieve a comprehensive comparison of their decay channels. To give a better and straightforward insight, the calculated half-lives of the four decay choices, namely α decay, heavier cluster emission, β decay, and spontaneous fission (SF), in uranium isotopes are plotted versus the mass number of parent nuclei in Fig. 1. From this figure, several interesting features about the decay pattern of U isotopes can be described as follows. (i) When the mass number is below about 230, α decay lies in the dominant position, the β decay and SF process seem to be comparable with each other and share a small part of the decay scheme, while the heavier cluster emission is the most impossible decay path. (ii) In the region around $A \sim 230$, α decay and β decay can be compatible and prevalent, and heavier cluster emission is closely competing with spontaneous fission. (iii) With increasing neutron number, β decay will be the governing decay mode for uranium isotopes, while α decay gradually holds a relatively smaller ratio of the decay channels and competes with SF in the extreme neutron-rich region. Heavier cluster emission still occupies a tiny decay share. (iv) In general, cluster decay is more common in the $A \sim 230$ region, leading to the doubly-magic daughter nucleus ^{208}Pb (or neighboring nuclei). Ultimately, a universal picture of decay characteristics has been built for uranium isotopes, as shown in Fig. 1.

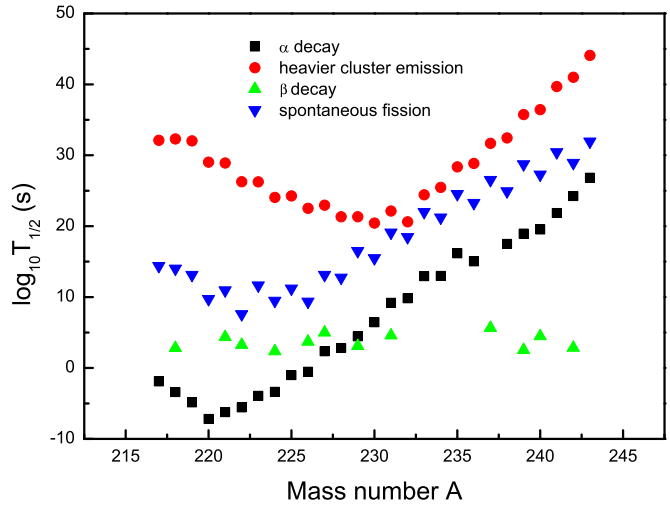

FIG. 1. Variation of calculated half-lives in different decay modes with the mass number of the parent nucleus for $^{217-243}$U. The black square denotes α decay, the red circle indicates heavier cluster emission, the green upward triangle means β decay, and the blue downward triangle represents spontaneous fission.

IV. SUMMARY

In summary, we further investigate α and heavier cluster decay of uranium isotopes with $217 \leqslant A \leqslant 243$ in an improved density-dependent cluster model, with special attention paid to the density distribution of target nuclei. Based on the excellent agreement between theory and experiment, systematic predictions on lifetimes of α decay and heavier cluster emission are made for U nuclides. Our calculated results are found to be compatible with other evaluations from proven formulas. Through the approximation of the nuclear transition matrix element, β decay half-lives are estimated by reducing to a Fermi function computation with respect to all kinds of β processes. Meanwhile, an effective relationship that connects the SF half-life to the fission barrier and fissility parameter has been employed to understand the general trend of spontaneous fission in U. By combining these, the decay behavior of uranium isotopes is fully determined from the theoretical side, which is hoped to serve as a valuable reference for future experiments.

ACKNOWLEDGMENTS

This work is supported by the National Natural Science Foundation of China (Grants No. 11375086, No. 11535004, No. 11605089, and No. 11120101005), by the Natural Science Youth Fund of Jiangsu Province (Grant No. BK20150762), by

the Fundamental Research Funds for the Central Universities (Grant No. 30916011339), by the 973 National Major State Basic Research and Development Program of China (Grant No. 2013CB834400), and by a Project Funded by the Priority Academic Programme Development of JiangSu Higher Education Institutions (PAPD).

[1] M. Wang, G. Audi, A. H. Wapstra, F. G. Kondev, M. MacCormick, X. Xu, and B. Pfeiffer, Chin. Phys. C **36**, 1603 (2012); G. Audi, F. G. Kondev, M. Wang, B. Pfeiffer, X. Sun, J. Blachot, and M. MacCormick, *ibid.* **36**, 1157 (2012).
[2] L. Ma, Z. Y. Zhang, Z. G. Gan, H. B. Yang, L. Yu, J. Jiang, J. G. Wang, Y. L. Tian, Y. S. Wang, S. Guo, B. Ding, Z. Z. Ren, S. G. Zhou, X. H. Zhou, H. S. Xu, and G. Q. Xiao, Phys. Rev. C **91**, 051302(R) (2015).
[3] H. B. Yang, Z. Y. Zhang, J. G. Wang, Z. G. Gan, L. Ma, L. Yu, J. Jiang, Y. L. Tian, B. Ding, S. Guo, Y. S. Wang, T. H. Huang, M. D. Sun, K. L. Wang, S. G. Zhou, Z. Z. Ren, X. H. Zhou, H. S. Xu, and G. Q. Xiao, Eur. Phys. J. A **51**, 88 (2015).
[4] J. Khuyagbaatar, A. Yakushev, Ch. E. Düllmann, D. Ackermann *et al.*, Phys. Rev. Lett. **115**, 242502 (2015).
[5] A.-P. Leppänen, J. Uusitalo, S. Eeckhaudt *et al.*, Eur. Phys. J. A **25**, 183, (2005).
[6] Z. Kalaninová, S. Antalic, F. P. Heßberger, D. Ackermann, B. Andel, B. Kindler, M. Laatiaoui, B. Lommel, and J. Maurer, Phys. Rev. C **92**, 014321 (2015).
[7] J. O. Rasmussen, Phys. Rev. **113**, 1593 (1959).
[8] B. Buck, J. C. Johnston, A. C. Merchant, and S. M. Perez, Phys. Rev. C **53**, 2841 (1996).
[9] P. R. Chowdhury, C. Samanta, and D. N. Basu, Phys. Rev. C **73**, 014612 (2006).
[10] D. N. Poenaru, I. H. Plonski, and W. Greiner, Phys. Rev. C **74**, 014312 (2006).
[11] D. N. Poenaru, R. A. Gherghescu, and W. Greiner, Phys. Rev. Lett. **107**, 062503 (2011).
[12] V. Yu. Denisov, Phys. Rev. C **88**, 044608 (2013).
[13] V. Yu. Denisov, O. I. Davidovskaya, and I. Yu. Sedykh, Phys. Rev. C **92**, 014602 (2015).
[14] P. Mohr, Phys. Rev. C **73**, 031301(R) (2006).
[15] G. Royer, Nucl. Phys. A **848**, 279 (2010).
[16] H. F. Zhang and G. Royer, Phys. Rev. C **77**, 054318 (2008).
[17] C. Xu, Z. Ren, and X. Zhang, J. Phys. G: Nucl. Part. Phys. **41**, 105106 (2014).
[18] K. P. Santhosh, J. G. Joseph, and B. Priyanka, Nucl. Phys. A **877**, 1 (2012).
[19] M. Ismail, A. Adel, and M. M. Botros, Phys. Rev. C **93**, 054618 (2016).
[20] M. Ismail, W. M. Seif, and A. Abdurrahman, Phys. Rev. C **94**, 024316 (2016).
[21] D. S. Delion, Monika Patial, R. J. Liotta, and R. Wyss, J. Phys. G: Nucl. Part. Phys. **43**, 095109 (2016).
[22] D. Ni, Z. Ren, T. Dong, and C. Xu, Phys. Rev. C **78**, 044310 (2008).
[23] Y. Ren and Z. Ren, Phys. Rev. C **85**, 044608 (2012).
[24] Y. Qian and Z. Ren, Phys. Rev. C **85**, 027306 (2012).
[25] S. Peltonen, D. S. Delion, and J. Suhonen, Phys. Rev. C **75**, 054301 (2007).
[26] D. Ni and Z. Ren, Ann. Phys. **358**, 108 (2015).
[27] Y. Qian and Z. Ren, J. Phys. G: Nucl. Part. Phys. **43**, 065102 (2016).
[28] Y. Qian, Z. Ren, and D. Ni, Phys. Rev. C **94**, 024315 (2016).
[29] A. V. Karpov and V. I. Zagerbaev, Int. J. Mod. Phys. E **21**, 1250013 (2012).
[30] X. Zhang and Z. Ren, Phys. Rev. C **73**, 014305 (2006).
[31] V. I. Zagrebaev, A. S. Denikin, A. V. Karpov, A. P. Alekseev, M. A. Naumenko, V. A. Rachkov, V. V. Samarin, and V. V. Saiko, NRV web knowledge base on low-energy nuclear physics, http://nrv.jinr.ru/.
[32] G. Bertsch, J. Borysowicz, H. Mcmanus, and W. G. Love, Nucl. Phys. A **284**, 399 (1977).
[33] G. R. Satchler and W. G. Love, Phys. Rep. **55**, 183 (1979).
[34] A. M. Kobos, B. A. Brown, P. E. Hodgson, G. R. Satchler, and A. Budzanowski, Nucl. Phys. A **384**, 65 (1982).
[35] K. Wildermuth and Y. C. Tang, *A Unified Theory of the Nucleus* (Academic Press, New York, 1997).
[36] R. J. Liotta, J. Phys.: Conf. Ser. **413**, 012012 (2013).
[37] D. Deng and Z. Ren, Phys. Rev. C **93**, 044326 (2016).
[38] H. F. Zhang, G. Royer, Y. J. Wang, J. M. Dong, W. Zuo, and J. Q. Li, Phys. Rev. C **80**, 057301 (2009).
[39] P. Möller, A. J. Sierk, T. Ichikawa, and H. Sagawa, At. Data Nucl. Data Tables **109-110**, 1 (2016).
[40] J. D. Walecka, *Theoretical Nuclear Physics and Subnuclear Physics* (Oxford University Press, Oxford, 1995), p. 11.
[41] B. Hahn, D. G. Ravenhall, and R. Hofstadter, Phys. Rev. **101**, 1131 (1956).
[42] D. Ni and Z. Ren, Phys. Rev. C **92**, 054322 (2015).
[43] A. Trzcińska, J. Jastrzębski, P. Lubiński, F. J. Hartmann, R. Schmidt, T. von Egidy, and B. Kłos, Phys. Rev. Lett. **87**, 082501 (2001).
[44] M. Warda, X. Viñas, X. Roca-Maza, and M. Centelles, Phys. Rev. C **81**, 054309 (2010).
[45] C. M. Tarbert, D. P. Watts, D. I. Glazier *et al.*, Phys. Rev. Lett. **112**, 242502 (2014).
[46] I. Angeli and K. P. Marinova, At. Data Nucl. Data Tables **99**, 69 (2013).
[47] S. Abrahamyan, Z. Ahmed, H. Albataineh *et al.*, Phys. Rev. Lett. **108**, 112502 (2012).
[48] NNDC of the Brookhaven National Laboratory, http://www.nndc.bnl.gov.